Journal of Energy Storage 55 (2022) 105343

Contents lists available at ScienceDirect

Journal of Energy Storage

journal homepage: www.elsevier.com/locate/est

Research papers

# Impact of micro-cycles on the lifetime of lithium-ion batteries: An experimental study

Adrian Soto, Alberto Berrueta, Miren Mateos, Pablo Sanchis, Alfredo Ursúa *

*Institute of Smart Cities (ISC), Department of Electrical, Electronic and Communications Engineering, Public University of Navarre (UPNA), Campus de Arrosadia, 31006 Pamplona, Spain*

ARTICLE INFO

*Keywords:*
Aging
Depth of discharge
Electric vehicle
Micro-cycle
Lithium-ion
Renewable energy

ABSTRACT

Experimental aging studies are commonly conducted on lithium-ion batteries by full charge and discharge cycles. However, such profiles may differ from the actual operation of batteries in electric vehicles and stationary applications, where they are subjected to different partial charges and discharges. These partial cycles, which take place during a main charge or discharge process, are called micro-cycles if their depth of discharge is <2 %. A number of authors have pointed out the relevance of the time resolution to estimate the energy throughput of a battery due to these micro-cycles in applications such as renewable microgrids. However, to the best of our knowledge, there are no experimental studies in the literature that assess the impact of these micro-cycles on battery degradation. In this article, the impact of micro-cycles on the loss of performance of a lithium-ion battery is experimentally studied. The results show that micro-cycles have a negligible, or even positive effect on the aging of lithium-ion cells compared to the aging caused by full cycles. In fact, if charge throughput or equivalent full cycles are used to measure the use of a battery, then cells subjected to micro-cycles exhibit a 50 % extended lifetime compared to cells only subjected to full cycles. More precisely, cells including micro-cycles with depth of discharge of 0.5 % lasted for nearly 3000 equivalent full cycles, whereas cells aged under standard deep cycles lasted for no >1500. Nevertheless, if the number of deep cycles, disregarding micro-cycles, is the unit to measure battery use, then the degradation of cells with and without micro-cycles is similar. Based on this result, the number of cycles can be identified as a more accurate variable to measure the use of a cell, in comparison to charge throughput.

## 1. Introduction

Combating climate change without abandoning the welfare state and industrial development is one of the most ambitious targets to date. In this regard, renewable energy generation and the electrification of transport are two significant challenges to be faced. Nevertheless, to envisage a future that moves away from dependency on fossil fuels, the development of energy storage systems is required, thereby making it possible for the energy produced from the variable renewable sources to be decoupled from power consumption. Due to their high energy density and great cyclability, lithium-ion batteries have been put forward as a feasible technology, both for electric vehicles (EV) and stationary applications [1–3].

However, the complex electrochemical reactions and structural changes that cause the aging of lithium-ion batteries are yet to be completely understood [4]. A great effort is being made to fully understand and predict the aging of lithium-ion batteries. It is well known that extrinsic factors such as temperature, current and voltage limits, among others, have a significant influence on the aging of the cells. Research studies aiming to identify the influence of such factors have been conducted at laboratory level under controlled conditions. Nevertheless, the standard aging profiles used by laboratories may differ from the actual operating profiles. Micro-cycles are a clear example of these different profiles.

Micro-cycles can be defined as a small swing in the state of charge (*SOC*) of <2 %, caused by the change of current sign during a greater charge or discharge of a battery, which implies a fast change in the polarization of the battery [5]. This is a common real phenomenon during battery operation, for batteries used in hybrid and full EV applications alike, as well as in stationary applications [6–8]. While driving an EV, the battery is discharged. However, the regenerative braking system charges the battery for short periods of time. Similarly, a battery used in a self-consumption installation tied to photovoltaic (PV)

* Corresponding author.
*E-mail address:* alfredo.ursua@unavarra.es (A. Ursúa).

https://doi.org/10.1016/j.est.2022.105343
Received 17 May 2022; Received in revised form 12 July 2022; Accepted 15 July 2022
Available online 8 August 2022

**Nomenclature**

| | |
|---|---|
| $C$ | charge capacity (Ah) |
| *C-rate* | current rate (C) |
| *DOD* | depth of discharge (%) |
| $E$ | energy capacity (Wh) |
| *EFC* | equivalent full cycle |
| *EOL* | end of life |
| $i$ | current (A) |
| $Q_R$ | relative electric charge (p.u.) |
| $R_{DC}$ | internal resistance (Ω) |
| *SOC* | state of charge (%) |
| *SOH* | state of health (%) |
| $t$ | time (h) |
| $V$ | constant voltage (V) |
| $v$ | terminal voltage (V) |

*Greek symbols*

| | |
|---|---|
| $\eta_E$ | round-trip energy efficiency (%) |

*Subscripts*

| | |
|---|---|
| *cell* | cell |
| *ch* | charge |
| cyc | cycle |
| *dch* | discharge |
| *i* | initial |
| e | end |
| *N* | nominal |

*Abbreviations*

| | |
|---|---|
| EV | electric vehicle |
| PV | photovoltaic |
| RPT | reference performance test |
| S | stage |

generation is charged when production is higher than demand. Subsequently, the battery is discharged when demand exceeds production. Variations in load and/or generation caused by passing clouds lead to short micro-cycles, particularly during sunlight hours.

Although micro-cycles are known to take place, previous publications have highlighted the fact that they are not always taken into account when sizing and predicting the lifetime of a battery, mainly due to the insufficient time resolution of the dataset or the large time step used in the simulations [9–13]. The total charge throughput of a battery in a standard renewable microgrid has been quantified to be around 14 % higher if it is calculated using data with a time resolution of 1 s compared to 1 h data [14], similar results can be found in further research works [15–17]. Therefore a battery aging model based on charge throughput estimates a longer lifetime with a time step in hours than with a time step in seconds.

Analogically, real driving conditions of electric vehicles include micro-cycles, while standard tests performed to assess aging are based on full charges and discharges [18–21]. Therefore, cell aging is commonly studied by including factors such as number of cycles, temperature, C-rate and *SOC*, while small micro-cycles are not taken into account [22–24]. C-rate, expressed in C, is defined as the measurement of the charge or discharge current with respect to its nominal capacity.

A number of studies optimizing battery use have been published in the last few years. These studies are based on cycle aging models including dependency on temperature, current and charge throughput among others [25,26]. These models are based on the fact that higher charge throughput causes faster aging for the same temperature and current. Such an assumption would lead to the conclusion that a cycle including micro-cycles, where the charge throughput is higher than in a standard cycle, would generate a higher capacity fade.

In this paper, the effect of micro-cycles and their width on the aging of lithium-ion cells is experimentally studied in eight 18,650 cells. With this aim, this paper is organized as follows. Section 2 offers a detailed explanation of the experimental setup; the effects of the micro-cycles on four of the main electrical parameters of a lithium-ion cell are presented in Section 3. In Section 4, the main results and findings are discussed and, finally, Section 5 summarizes the main results and sets out the conclusions.

## 2. Experimental setup

### 2.1. General description of the test bench

Eight LG 18650HG2 cells with a nominal capacity of $C_N = 3$ Ah and an energy capacity of $E_N = 11$ Wh are tested in this study to analyze the influence of micro-cycles. The cells, as declared by the manufacturer, have a graphite + SiO anode, an H-NMC based cathode and a nominal voltage $V_N = 3.6$ V. The operating voltage of the cells ranges from 2.5 V to 4.2 V. As explained in the following subsections, the cells are cycled under different profiles, and recurrent reference performance tests (RPTs) are conducted to monitor the characteristics of the cells. All the tests were conducted at the Laboratory for Energy Storage and Microgrids of the Public University of Navarre in an Ineltec −30/300 thermal chamber at a controlled temperature of 20 °C ± 0.5 °C and using a Neware BTS4016-5V battery tester having a voltage and current precision of ±0.1 % of the scale. Moreover, the four-terminal sensing method was used to ensure the proper measurement at cell terminal and the surface temperature of the cells was constantly monitored, as shown in Fig. 1.

### 2.2. Aging test matrix

The aging experiments presented herein are designed to suit typical battery operation profiles relating to renewable energy systems. For this purpose, the cyclability of the battery of a typical self-consumption installation is analyzed, and the test matrix is designed accordingly.

The Rainflow algorithm can be used to determine the battery cyclability. The Rainflow algorithm makes it possible to identify and account half or full cycles within an irregular load profile [27]. Although the algorithm has its origin in mechanics for fatigue analysis, it is widely

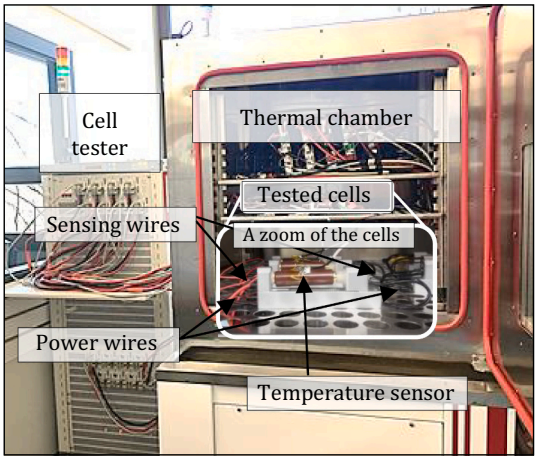


**Fig. 1.** A picture of the test bench located at the Laboratory for Energy Storage and Microgrids of the Public University of Navarre.

applied for accounting cycles during real operation of lithium-ion batteries [28,29]. Fig. 2 shows the result provided by such algorithm in the operation of a 3.3 kWh lithium-ion battery at the self-consumption installation located in the northern Spain (42°48′00.6″N 1°38′04.4″W) operating for 52 weeks [14]. Whereas the battery was subjected to around 1 deep discharge cycle per day (from the minimum allowed 10 % *SOC* to maximum 95 %), several micro-cycles (DOD < 2 %) were recorded during the year. As represented in Fig. 2 >30,000 cycles of DOD ≤ 0.5 % took place, those micro-cycles have their origin in the household variable power consumption and/or PV generation. During that period, the battery was submitted to 285 cycles of DOD > 80 %. The depth of discharge (DOD) of a cycle represents the charge throughput during the cycle divided by two times the nominal capacity, as expressed in Eq. (1).

$$DOD = \frac{100}{2 \cdot C_N} \cdot \int_{t_{i,cyc}}^{t_{e,cyc}} |i_{cell}(t)| \cdot dt \tag{1}$$

where $i_{cell}$ is the cell current, $t_{i,\,cyc}$ is the initial time and $t_{e,\,cyc}$ the ending time of the cycle. Due to the large number of micro-cycles, it is necessary to correctly address the actual impact of these small micro-cycles on the aging of a lithium-ion battery.

In view of this, a test matrix including the effect of the most recurrent micro-cycles was designed, consisting in four experiments, each with two samples. The four experiments are described below and summarized in Table 1.

Micro-cycles consist in a reversed current followed by a subsequent polarity change during the required time to achieve the desired DOD. Since in both phases, the elapsed time and current is the same, the stored electric charge at the beginning and at the end of the micro-cycle remains invariant as schematically represented in Fig. 3, being $Q_R$ the charge available in a cell related to the storable charge throughout the aging test. State of health (*SOH*) is defined as expressed by Eq. (2), and the end of life (EOL) criteria is set as *SOH* < 75 %.

$$SOH = 100 \cdot \frac{C}{C_i} \tag{2}$$

where $C$ is the current charge capacity and $C_i$ is the initial capacity. Charges and discharges between the voltage limits were performed by the constant current method without a constant voltage phase so as the current amplitude was constant throughout all the experiment. Given that the current as well as the ambient temperature in all cells are constant, the only difference in the aging of the cells can be attributed to the micro-cycles and to manufacturing inhomogeneities.

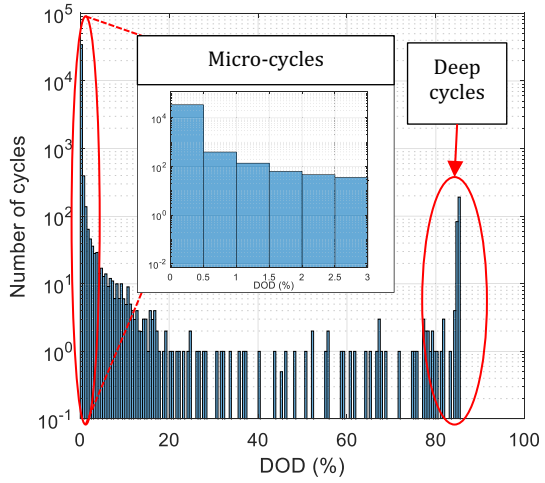


**Fig. 2.** Number of cycles per depth of discharge (DOD) obtained for a self-consumption installation during 52 weeks of operation.

**Table 1**
Micro-cycle test matrix.

| # | Micro-cycle DOD (%) | Cell N | Identifier | Duration of main process (s) | Duration of micro-cycle (s) |
|---|---|---|---|---|---|
| *i*) | 0 % | 1 | ● | – | – |
| | | 2 | ▲ | | |
| *ii*) | 0.5 % | 3 | ● | 54 | 36 |
| | | 4 | ▲ | | |
| *iii*) | 1 % | 5 | ● | 108 | 72 |
| | | 6 | ▲ | | |
| *iv*) | 2 % | 7 | ● | 216 | 144 |
| | | 8 | ▲ | | |

*i*) Continuous deep charge – discharge cycles with a current of 3 A (1C) between the minimum and maximum allowed voltage (2.5–4.2 V).
*ii*) Deep charge – discharge cycles with the same current and voltage limits, with continuous superimposed micro-cycles with DOD = 0.5 %.
*iii*) Deep charge – discharge cycles with the same current and voltage limits, with continuous superimposed micro-cycles with DOD = 1 %.
*iv*) Deep charge – discharge cycles with the same current and voltage limits, with continuous superimposed micro-cycles with DOD = 2 %.

### 2.3. Reference performance test (RPT)

RPTs are of the utmost importance during aging tests, given that they provide accurate information concerning cell degradation and performance. Nevertheless, their impact on the aging test should be minimized. With this aim, the following RPT is proposed.

1) Discharge the cell to its minimum voltage at a current of 1 A (C/3).
2) Charge it to its maximum voltage at a current of 1 A (C/3), followed by a constant-voltage stage to a cut-off current of 0.12 A (C/25).
3) Discharge it with a current of 1 A (C/3) to the minimum voltage.
4) Galvanostatically charge the cell by pulses of $\Delta SOC$ = 20 %, with a current of 1 A.
5) Let the cell rest for 1 h after each galvanostatic charge.

The current charge capacity ($C$) and energy capacity ($E_{dch}$) are calculated from the measurements in step 3, and the round-trip energy efficiency ($\eta_E$) is calculated from steps 2 and 3. The low current of C/3 prevents the self-heating of the cell, allowing accurate capacity measurement [30]. Note that capacity tests were conducted at C/3 whereas the aging tests were performed at 1C. Finally, five internal resistance ($R_{DC}$) calculations are done with the data measured in steps 4 and 5.

## 3. Effect of micro-cycles on the performance of lithium-ion cells

The performance of a Li-ion battery can be described by a number of performance indicators. The four indicators analyzed in this paper obtained by the RPT described above are: $C$, $E_{dch}$, $\eta_E$ and $R_{DC}$. $C$ can be defined as the amount of charge that can be stored in a cell under specified conditions, whereas $E_{dch}$ represents the amount of energy. These two parameters are closely related, but they can offer supplementary information. $\eta_E$, as described by Eq. (3) is defined as the ratio between the discharged and charged energy during a cycle.

$$\eta_E = \frac{E_{dch}}{E_{ch}} \tag{3}$$

The internal resistance, which is a compendium of the ohmic resistance, the activation overpotential and the diffusion effects, is obtained from a current pulse with a duration of 10 s. $R_{DC}$ can be calculated from Ohm's law, as represented by Eq. (4).

$$R_{DC} = \frac{\Delta v}{\Delta i_{cell}} \tag{4}$$

being $\Delta i_{cell}$ the current pulse, and $\Delta v$ the voltage response of the battery 10 s after the current pulse.

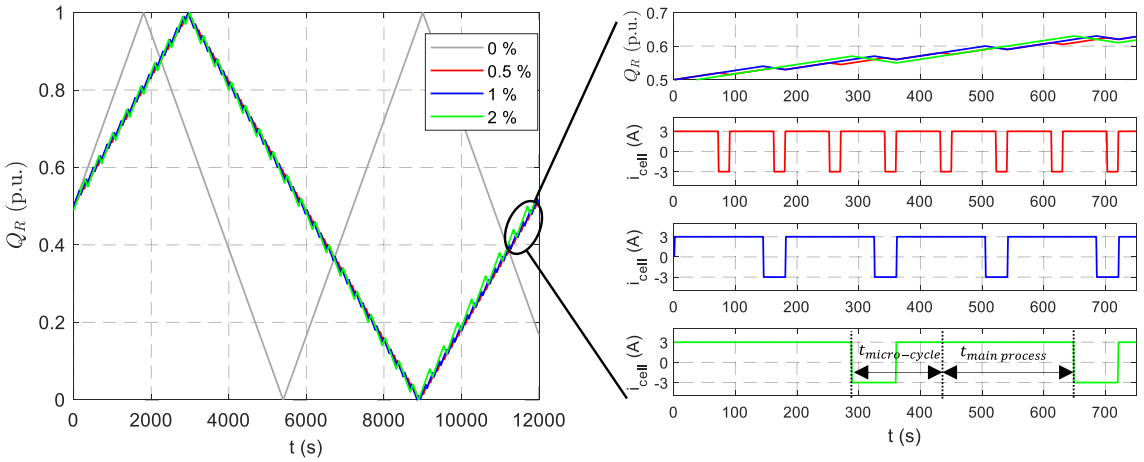


**Fig. 3.** Aging profiles of the cells: without micro-cycles in gray, micro-cycles of 0.5 % DOD in red, of 1 % DOD in blue and of 2 % DOD in green. (For interpretation of the references to color in this figure legend, the reader is referred to the web version of this article.)

These performance indicators are analyzed throughout the cell lifetime. Given that all cells are cycled for the same time, at the same temperature and average voltage, the calendar aging is considered similar in all cells, and the analysis is thus focused on cycle lifetime. The most detailed approach to quantify the cycle aging is to calculate the number of cycles at each DOD using the Rainflow algorithm. The cycle profiles analyzed in this article (see Table 1) are built by micro-cycles superimposed on deep cycles. Another alternative, that provides an overall number to quantify the battery cyclability, is equivalent full cycles (*EFC*). An *EFC* is defined as the number of times that the charge throughput of a cell is twice its nominal capacity, as represented by Eq. (5).

$$EFC = \frac{\int_{t_0}^{t_1} \left| i_{cell}(t) \right| \cdot dt}{2 \cdot C_N} \tag{5}$$

The following four subsections show the effect of the different cell cyclabilities described in Table 1 over each of the four performance indicators. The marker and color used to identify each cell is also compiled in Table 1. Each analysis is presented in two figures, in order to show the variation in the result achieved by each counting method (deep cycles and *EFC*). Moreover, all the performance indicators except *C* are represented in terms of *SOH*.

### 3.1. Charge capacity

The *SOH* as described by Eq. (2) is used to uniformly express the charge capacity fade of a cell. Fig. 4 shows the *SOH* of the eight cells during the experiment. The *SOH* fade can be divided into four stages, based on the fade rate. During the first stage (SI), the solid – electrolyte interface (SEI) at the graphitic anode is formed by the irreversible decomposition of the electrolyte, causing a sharp capacity fade. In the second stage (SII), the internal states of the cells gradually stabilize and the capacity fade gradient is reduced [24]. Below an *SOH* of 80 %, the capacity fade reaches a plateau region due to a stabilization in the side reactions causing the continuous growth of the SEI, structural transformation of the cathode and the loss of electrolyte [31], and leading to the third stage (SIII) until the EOL (*SOH* = 75 %) is reached. At the EOL an aging knee is observed at the start of the fourth stage (SIV). SIV has been put forward as a promising solution for the reutilization of batteries coming from electric vehicles, giving them a second life and encouraging the circular economy [18]. In SIV a rapid capacity drop and resistance rise is caused by the enhanced loss of lithium ion inventory resulting in lithium plating, volumetric changes at the anode and binder failure causing the contact loss of active material at the electrodes [31].

If the capacity fade of the eight cells is compared in terms of deep cycles, as shown in Fig. 4(a), no noteworthy difference among them is measured, irrespective of whether or not the cells are subjected to micro-cycles. Beyond the EOL a larger dispersion is measured, even for cells

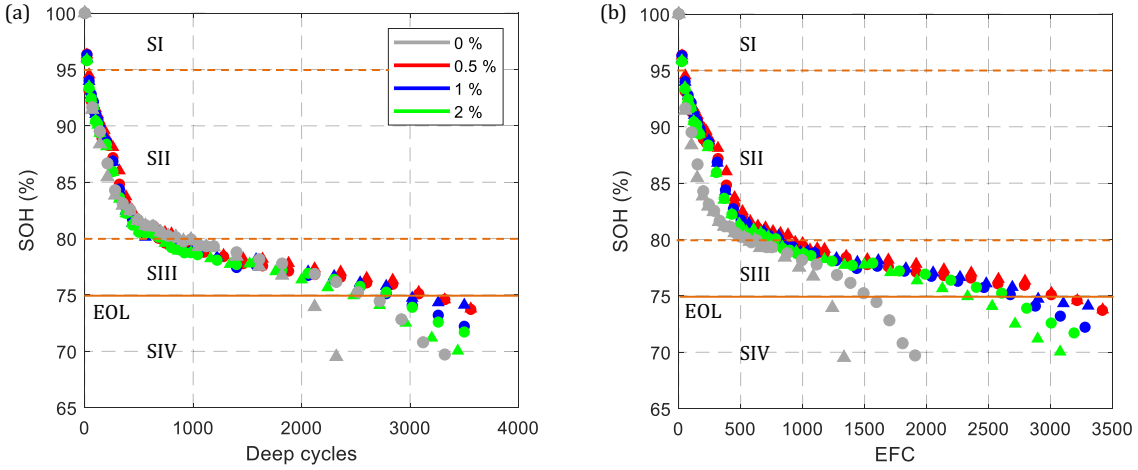


**Fig. 4.** Capacity fade of the 8 cells expressed as *SOH*: (a) *SOH* as function of deep cycles and (b) *SOH* as function of *EFC*.

having the same cycle profile. This effect can be attributed to the larger impact of manufacturing inhomogeneities at this advanced degradation of the cells. The greatest difference between cells with the same cycle profile is between cells 1 and 2, whose lifespans differ in almost 575 deep cycles. The reduced lifetime of cell 2 presumably can be linked to manufacturing inhomogeneities. The differences among the other pairs of cells cycled under the same profile are 41 deep cycles for cells 3 and 4, 150 for cells 5 and 6, and 360 for cells 7 and 8. Even though, all cells apart from cell 2 show a similar capacity fade in terms of deep cycles, cells subjected to micro-cycles of 0.5 % exhibited an extended lifespan in comparison with the rest. Cells managing micro-cycles of 1 % withstand more deep cycles than cells that include micro-cycles of 2 %, which lasted approximately the same number of deep cycles as cell 1, which was cycled without micro-cycles.

Comparing homogeneous aging among the seven cells reported, if the number of deep cycles is taken as the cycle quantification, a great difference between the cells with micro-cycles and those without micro-cycles can be observed if *EFC* are used as cycle counting variables, as shown in Fig. 4(b). The mismatch becomes noticeable from the beginning of the test and increases until EOL is reached. The difference measured in the cycle life of cells with and without micro-cycles ranges from 711 *EFC* to 1513 *EFC* (note that cell 2 has been reported to be defective).

An analysis of Fig. 4 shows that the cycle lifetime of cells with and without micro-cycles is similar if the correct cycle counter is used. These results demonstrate that the number of cycles (excluding micro-cycles) is a more suitable cycle counter than *EFC*. Therefore, this analysis leads to two results. Firstly, that for smaller micro-cycles the cycle life of a Li-ion cell is slightly longer. Secondly, that an ampere hour counting method for the cyclability of a battery should be able to identify micro-cycles, given that an aggregated battery cyclability that includes deep cycles and micro-cycles would lead to an incorrect interpretation as shown in Fig. 4(b).

### 3.2. Energy capacity

Fig. 5(a) and (b) show the energy capacity decay in terms of deep cycles and *EFC*. The dispersion reported in the previous subsection regarding *SOH* fade is also evident in the energy capacity fade. Specifically, the aging observed in cells with micro-cycles appears to be lower if cell use is accounted for by *EFC*. Therefore, the same conclusion concerning the unsuitability of *EFC* as a variable to account for battery cyclability is drawn from this analysis.

Fig. 5(c) shows an apparently linear relationship between energy capacity and *SOH*, independent of the aging profile of the cell, including the SEI formation stage (SI) and beyond the aging knee. The relationship between energy capacity and *SOH*, defined as charge capacity retention, is actually the discharge voltage of the cell ($V_{dch} = E_{dch}/C$). In order to have a detailed insight into this relationship, Fig. 6 shows the discharge

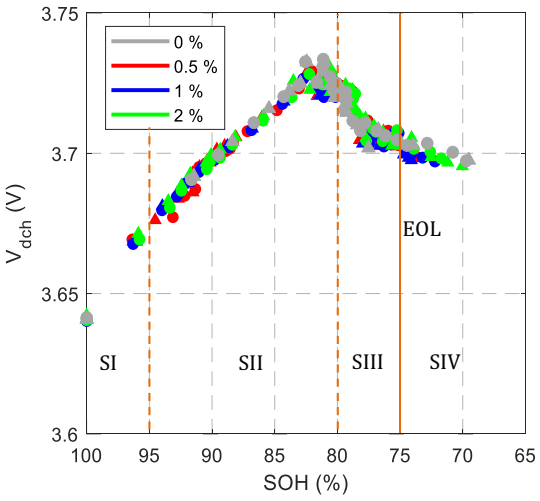


**Fig. 6.** Discharge voltage of the eight cells as function of *SOH*.

voltage of the cells for each *SOH*. $V_{dch}$ rises during SI and SII, and drops in SIII and SIV. This observation suggests that during the first two stages aging mechanisms affecting capacity fade are more significant than power fade aging mechanisms. In this regard, power fade is linked to greater internal resistance. Several degradation mechanisms take place simultaneously during the aging of Li-ion cells and can have a different impact on capacity fade or power fade [23], however, the identification of the undergoing mechanisms is outside the scope of this study. The reduced scattering observed in Fig. 6 proves that the discharge voltage and, therefore, the energy capacity, can be expressed uniquely in terms of *SOH*, irrespective of whether or not the aging profile is subjected to micro-cycles. Therefore, the result obtained for the *SOH* defined by means of the charge capacity is similar to the energy capacity fade of a Li-ion cell.

### 3.3. Round-trip energy efficiency

Round-trip efficiency during cycling is represented in Fig. 7(a), (b) and (c) as a function of *SOH*. During SI and SII the round-trip efficiency is not modified as the cells age. The wide scattering among the measurements is larger than any aging trend. However, for SIII, round-trip efficiency shows a linear decrease as a function of *SOH*. Finally, a sharp reduction in $\eta_E$ is recorded during SIV irrespective of the cycle counting method. A reduction in efficiency is commonly related to an increase in the internal resistance, thus a noticeable increase in the internal resistance is expected for SIII and SIV.

With regard to the effect of the micro-cycles on $\eta_E$, no clear correlation is evident in Fig. 7. The cells studied in this article provide a high

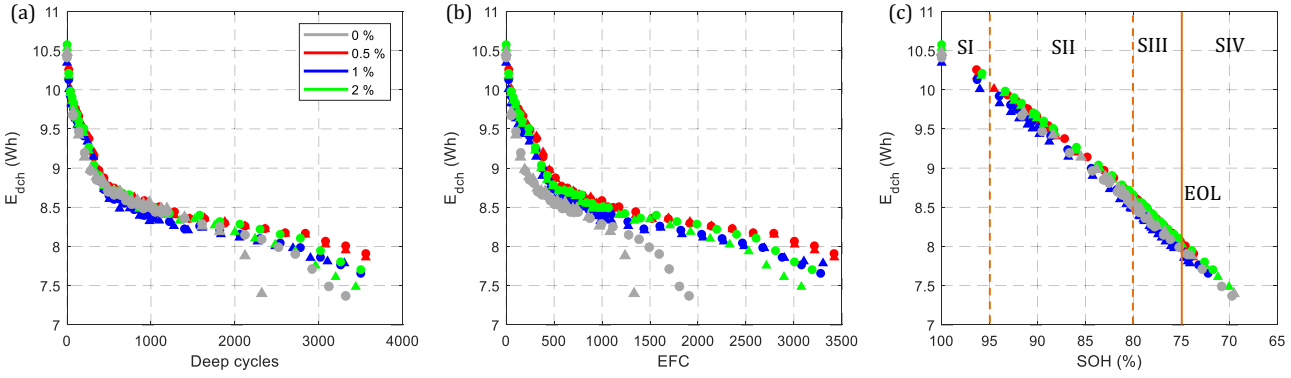


**Fig. 5.** Energy capacity fade of the 8 cells during cycling: (a) $E_{dch}$ as function of deep cycles, (b) $E_{dch}$ as function of *EFC* and (c) $E_{dch}$ as function of *SOH*.

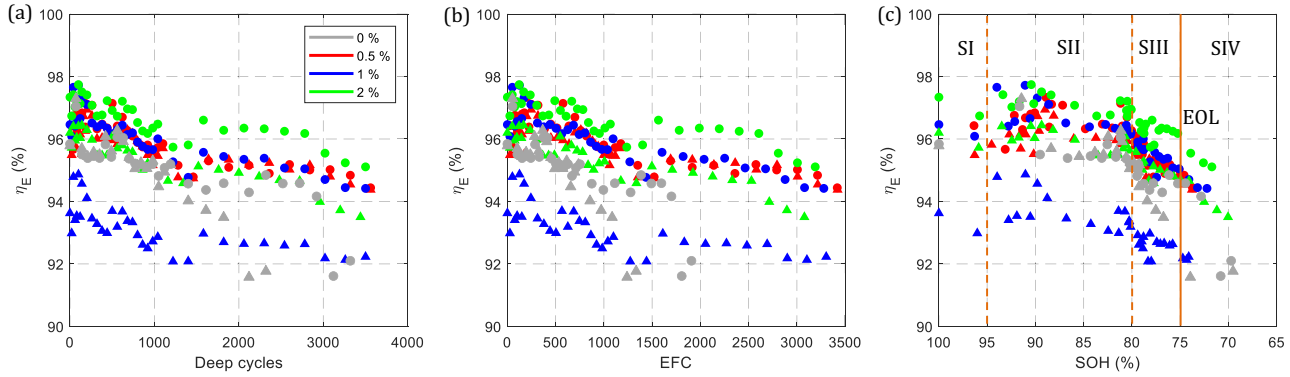


**Fig. 7.** Round trip efficiency of the 8 cells throughout cycling: (a) $\eta_E$ as function of deep cycles, (b) $\eta_E$ as function of *EFC* and (c) $\eta_E$ as function of *SOH*.

energy efficiency, ranging from 94 % to 98 %, until the aging knee is reached. At EOL the cells maintain an efficiency of nearly 92 %. The efficiency of cell 6 is 2 % less than the remaining cells, which is attributed to manufacturing inhomogeneities.

### 3.4. Internal resistance

The internal resistances $R_{DC}$ obtained for *SOC* of 40 % and 60 % are shown in Fig. 8. During SI, $R_{DC}$ is reduced at both *SOC*, which can be related to the SEI layer formation during these cycles [32]. During SII, $R_{DC}$ increased at a small rate, as shown in Fig. 8(c) and (f). In SIII, starting at a *SOH* of 80 %, a sharp variation in $R_{DC}$ is observed, which is attributed to an increase in the charge transfer resistance at the electrodes. Finally, in SIV, after reaching EOL, $R_{DC}$ increases with a lower slope than the one observed in SIII. This trend is in line with the results presented in Sections 3.2 and 3.3 where the power fade and therefore $R_{DC}$ growth is identified as predominant at SIII and SIV.

Aligned with the conclusion about capacity fade drawn from Fig. 4, the internal resistance rise is similar, irrespective of the cell micro-cycle profile, if *SOH* is taken as an independent variable, while a significant difference emerges if *EFC* is taken as an independent variable between the cells with no micro-cycles and the remaining cells with micro-cycles. Therefore, these measurements show that the structural changes caused by the degradation mechanisms exhibit no significant correlation with the micro-cycles. The trends presented in this section are observed in $R_{DC}$ at the five measured *SOC*, even though only *SOC* 40 % and 60 % are included in Fig. 8 due to space limitations.

## 4. Effect of micro-cycles on the lifetime of lithium-ion cells and discussion

Predicting the lifetime of a lithium-ion battery is of pivotal importance for many applications. In such applications, the battery operating profile should be characterized in detail. For instance, as already

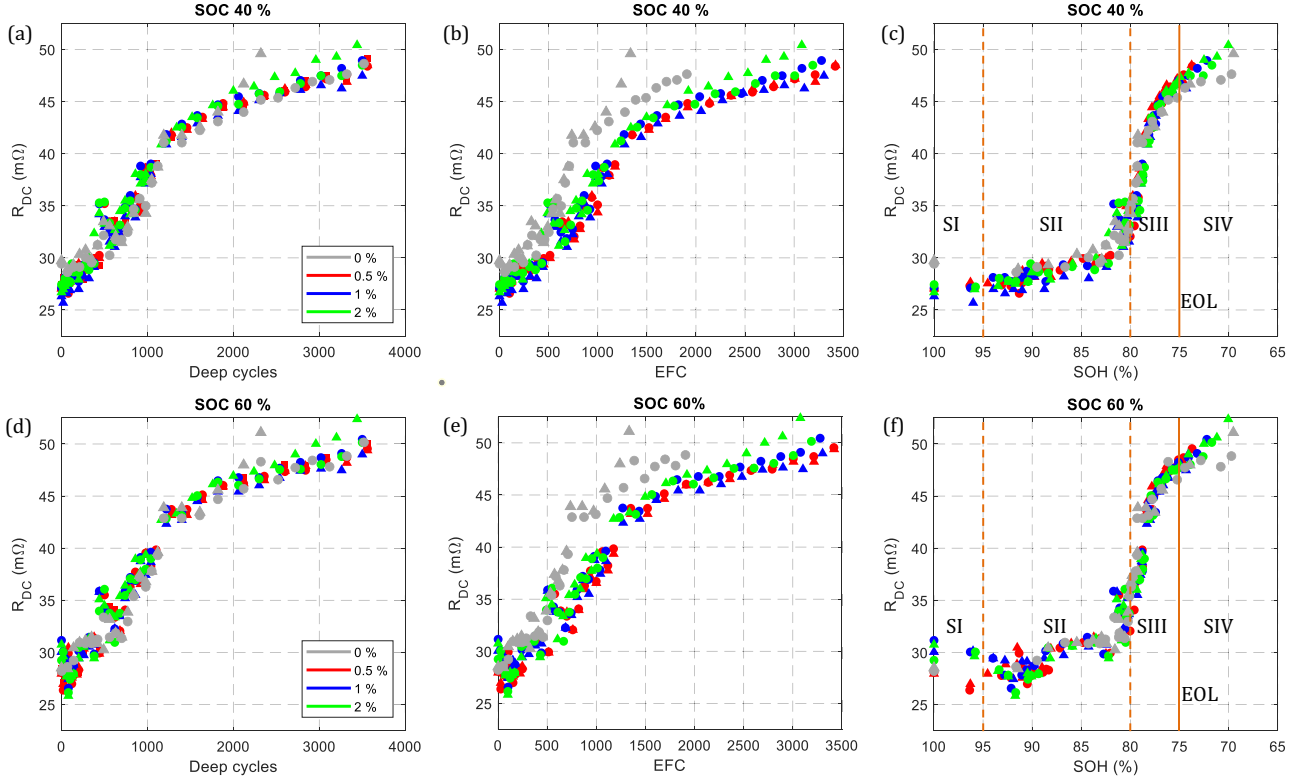


**Fig. 8.** $R_{DC}$ measurements in the eight tested cells, represented using number of deep cycles, EFC and *SOH*, respectively, as independent variable: (a), (b), (c)for *SOC* = 40 % and (d), (e), (f) for *SOC* = 60 %.

indicated herein, during the operation of an EV or a battery tied to a renewable-energy system, different micro-cycles take place. However, the aging information provided by the battery manufacturer is commonly based solely on the number of full charge and discharge cycles. In contrast, the most relevant parameter for an EV is the number of miles that have been driven before reaching EOL; while in most self-consumption systems the critical variable is the self-consumption ratio, which is related to the total charge throughput delivered during the battery lifetime. Since the real operation of a battery usually consists of partial charges and discharges, the use of the battery is often expressed in terms of *EFC*, which can be easily calculated as stated in Eq. (5).

Fig. 9 shows the *EFC* that each cell has been subjected to before reaching EOL, making a distinction between deep cycles and micro-cycles with different DOD. The experimental uncertainty due to the cumulative imprecisions of the current measurement is also in Fig. 9. The EFCs were accounted by decomposing the cycling profile in deep cycles and micro-cycles, conversely to the superposition presented in Fig. 3. The irregular cycle counting can be performed by means of an algorithm as the Rainflow. Thus, the cyclability of the cells can be compared in terms of 1) *EFC* coming from micro-cycles, 2) *EFC* caused by deep cycles, and 3) total *EFC* of the cells. In the case of cell 1 and 2, since there are no micro-cycles, the total use of the cells corresponds to deep cycles.

If the *EFC* caused merely by micro-cycles are considered, then cells 3 and 4 are subjected to 1192 and 1208 respectively, with 1033 and 1096 for cells 5 and 6, whereas cells 7 and 8 manage 975 and 857 *EFC* respectively. On average, cells having micro-cycles of 0.5 % DOD are able to manage 136 *EFC* more than those with micro-cycles of 1 %, and 293 more *EFC* than cells with micro-cycles of 2 %. This result agrees with previous studies that prove that cycles with lower DOD increase the cyclability of Li-ion cells [33].

Nevertheless, if the cell performance is compared in terms of *EFC* linked to deep cycles (gray area in Fig. 9), it can be observed that cells including micro-cycles of 0.5 % and 1 % are able to perform more *EFC* than cells with no micro-cycles. Meanwhile, cells including 2 % micro-cycles have approximately the same lifespan as cell 1, with no micro-cycles. These results suggest that micro-cycles with DOD $\leq$ 1 % are beneficial for the performance of the graphite + NMC Li-ion cells studied in this article, given that a higher number of deep cycles can be achieved before reaching EOL. Finally, as presented in Section 3.1, cells managing micro-cycles deliver between 711 and 1513 *EFC* more than cell 1, with no micro-cycles. This means an extended lifetime of 50.2 % for cell 4 and 31.9 % for cell 8, as can be calculated from Fig. 9. The results show that the cells subjected to micro-cycles present an extended lifespan in terms of *EFC*, which is in fact the most significant criteria concerning battery durability. Hence, a profile including partial charges and discharges caused by micro-cycles is more beneficial for a Li-ion cell than full charges and discharges. For instance, these results suggest that a battery of an EV with regenerative braking can last for more miles than a battery subjected only to deep cycles.

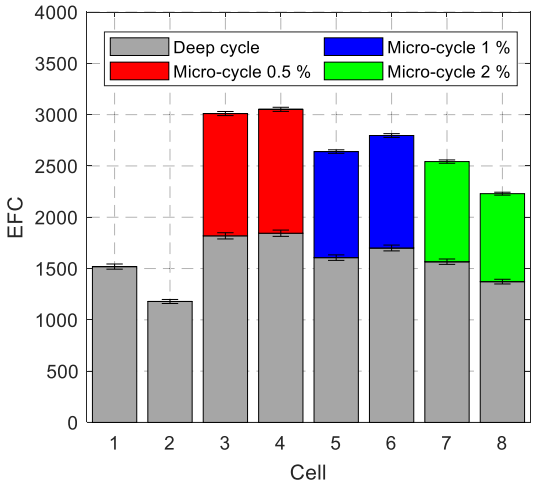


**Fig. 9.** Cycles before reaching EOL accounted by means of *EFC*.

The EOL of a battery can be calculated in terms of either *EFC* or deep cycles from the information provided on the battery datasheet. Most datasheets provide aging information obtained from experiments using charge/discharge profiles such as the one applied in this paper in cells 1 and 2. Based on this information, the lifespan of a battery could be predicted by means of the *EFC* characterized for its expected operation. In fact, the results presented in this study show that the cells subjected to micro-cycles have an extended lifespan in terms of *EFC*. The underestimation of the lifespan of a battery with a large number of micro-cycles can range from 31.9 % to 50.2 %. By contrast, if the number of deep cycles is used as an aging measurement, then the deviation is reduced to 5.3 % –measured between cell 1 and cell 4– to 18.1 % –measured between cell 1 and cell 8–. Similarly, as mentioned above, micro-cycles occurring in a self-consumption facility are disregarded as the time resolution of a simulation is increased, which leads to an underestimation of the number of *EFC*. A simple aging method based on *EFC* would provide a longer battery life estimation if the selected time step for the analysis is increased. Therefore, an intuitive approach to lifetime estimation would reduce the simulation step as much as possible, in order to account for the micro-cycles that are disregarded with longer time steps. However, the results presented in this article show that these micro-cycles have a negligible (DOD = 2 %) or even a positive (DOD $\leq$ 1 %) effect over capacity fade (Fig. 4) and internal resistance increases (Fig. 8). Therefore, if the aging model is fitted by means of aging tests with standard deep cycles, then the capacity fade should be expressed in terms of deep cycles, not *EFC*. In the same way, a time resolution that considers only deep cycles is suitable for predicting the lifetime of a battery.

For the applicability of these results to the analysis of a real battery operation, the standard aging profile consisting of full charges and discharges needs to be extrapolated to analyze real operation profiles with a considerable proportion of micro-cycles. To do so, a typical approach based on *EFC* or ampere counting is proved to be unsuitable for this extrapolation. Cycle counting methods, such as the Rainflow algorithm, are put forward as a more suitable solution for estimating the *SOH* of lithium-ion batteries, allowing the distinction between deep cycles and micro-cycles. The correlation observed between energy capacity, nominal voltage, round-trip efficiency and internal resistance with *SOH*, show a reduced effect of micro-cycles on the degradation mechanisms of Li-ion batteries. Therefore, the aging of Li-ion batteries is caused mainly by deep charge-discharge cycles.

## 5. Conclusions

It is widely agreed that larger charge throughput leads to faster aging and subsequent end-of-life of a lithium-ion battery, assuming constant ambient temperature and current rate. However, we have experimentally demonstrated in this paper that a larger charge throughput may not lead to faster aging. The results presented in this paper show that cells that are also subjected to micro-cycles are able to withstand a higher amount of *EFC* than cells under charge and discharge profiles that do not include micro-cycles. The lifespan was increased in the range of 31 % to 50 %. Moreover, the results indicate that microcycles of DOD $\leq$ 1 % have a positive influence on the lifespan of Li-ion cells.

Given that micro-cycles occur in real operation, but are not part of the standard aging tests performed in laboratories to characterize battery degradation, DOD is not always included in aging models. An aging model based on *EFC* counting would underestimate the real lifespan of a lithium-ion cell subjected to micro-cycles by 31 % to 50 %. Therefore, predicting and expressing the *SOH* of a battery in terms of number of

cycles, excluding micro-cycles, is pointed out as a more suitable alternative than the energy throughput or *EFC*.

## CRediT authorship contribution statement

**Adrian Soto:** Conceptualization, Methodology, Software, Formal analysis, Investigation, Visualization, Data curation, Writing – original draft. **Alberto Berrueta:** Conceptualization, Methodology, Investigation, Validation, Writing – review & editing. **Miren Mateos:** Methodology, Investigation, Validation. **Pablo Sanchis:** Conceptualization, Resources, Supervision, Project administration, Funding acquisition. **Alfredo Ursúa:** Conceptualization, Methodology, Writing – review & editing, Resources, Supervision, Project administration, Funding acquisition.

## Declaration of competing interest

The authors declare that they have no known competing financial interests or personal relationships that could have appeared to influence the work reported in this paper.

## Data availability

The data that has been used is confidential.

## Acknowledgements

This work is part of the projects PID2019-111262RB-I00, funded by MCIN/AEI/10.13039/501100011033/, STARDUST (774094), funded by European Union's Horizon 2020 research and innovation programme, HYBPLANT (0011-1411-2022-000039), funded by Government of Navarre, and a Ph.D. scholarship, funded by Public University of Navarre. Open access funding provided by Universidad Pública de Navarra.

## References

[1] A. Soto, A. Berrueta, I. Oficialdegui, P. Sanchis, A. Ursúa, Noninvasive aging analysis of lithium-ion batteries in extreme cold temperatures, IEEE Trans. Ind. Appl. 58 (2022) 2400–2410.
[2] X. Li, J. Zhao, J. Duan, S. Panchal, J. Yuan, R. Fraser, M. Fowler, M. Chen, Simulation of cooling plate effect on a battery module with different channel arrangement, J. Energy Storage. 49 (2022), 104113.
[3] A.R. Bais, D.G. Subhedar, S. Panchal, Critical thickness of nano-enhanced RT-42 paraffin based battery thermal management system for electric vehicles: a numerical study, J. Energy Storage 52 (2022), 104757.
[4] A. Wang, S. Kadam, H. Li, S. Shi, Y. Qi, Review on modeling of the anode solid electrolyte interphase (SEI) for lithium-ion batteries, Npj Comput. Mater. 4 (2018) 15.
[5] N. Narayan, T. Papakosta, V. Vega-Garita, J. Popovic-Gerber, P. Bauer, M. Zeman, A simple methodology for estimating battery lifetimes in Solar Home System design, in: 2017 IEEE AFRICON: Science, Technology and Innovation for Africa 2017, AFRICON, 2017, pp. 1195–1201.
[6] M. Ceraolo, G. Lutzemberger, D. Poli, Aging evaluation of high power lithium cells subjected to micro-cycles, J. Energy Storage 6 (2016) 116–124.
[7] M. Dubarry, A. Devie, Battery durability and reliability under electric utility grid operations: representative usage aging and calendar aging, J. Energy Storage. 18 (2018) 185–195.
[8] G. Baure, M. Dubarry, Battery durability and reliability under electric utility grid operations: 20-year forecast under different grid applications, J. Energy Storage 29 (2020), 101391.
[9] T. Beck, H. Kondziella, G. Huard, T. Bruckner, Assessing the influence of the temporal resolution of electrical load and PV generation profiles on self-consumption and sizing of PV-battery systems, Appl. Energy 173 (2016) 331–342.
[10] A. Berrueta, A. Soto, J. Marcos, I. De La Parra, P. Sanchis, A. Ursúa, Identification of critical parameters for the design of energy management algorithms for li-ion batteries operating in PV power plants, IEEE Trans. Ind. Appl. 56 (2020) 4670–4678.
[11] L. Millet, A. Berrueta, M. Bruch, N. Reiners, M. Vetter, Extensive analysis of photovoltaic battery self-consumption: evaluation through an innovative district case-study, Appl. Phys. Rev. 6 (2019), 021301.
[12] A. Ayala-Gilardón, M. Sidrach-de-Cardona, L. Mora-López, Influence of time resolution in the estimation of self-consumption and self-sufficiency of photovoltaic facilities, Appl. Energy 229 (2018) 990–997.
[13] P. Wolf, J. Včelák, Simulation of a simple PV system for local energy usage considering the time resolution of input data, J. Energy Storage 15 (2018) 1–7.
[14] A. Soto, A. Berrueta, P. Sanchis, A. Ursúa, Influence of renewable power fluctuations on the lifetime prediction of lithium-ion batteries in a microgrid environment, in: 2019 IEEE International Conference on Environment and Electrical Engineering and 2019 IEEE Industrial and Commercial Power Systems Europe (EEEIC/I&CPS Europe), 2019, pp. 1–6.
[15] A. Burgio, D. Menniti, N. Sorrentino, A. Pinnarelli, Z. Leonowicz, Influence and impact of data averaging and temporal resolution on the assessment of energeticEconomic and Technical Issues of Hybrid Photovoltaic-Battery Systems, Energies 13 (2020) 354.
[16] G. Brusco, A. Burgio, D. Menniti, M. Motta, A. Pinnarelli, N. Sorrentino, N. Tutkun, The time resolution of the load profile and its impact on a photovoltaic-battery system, in: 2018 IEEE International Conference on Environment and Electrical Engineering and 2018 IEEE Industrial and Commercial Power Systems Europe (EEEIC/I&CPS Europe), 2018, pp. 1–6.
[17] A. Ruddell, A. Dutton, H. Wenzl, C. Ropeter, D. Sauer, J. Merten, C. Orfanogiannis, J. Twidell, P. Vezin, Analysis of battery current microcycles in autonomous renewable energy systems, J. Power Sources 112 (2002) 531–546.
[18] E. Braco, I. San Martín, A. Berrueta, P. Sanchis, A. Ursúa, Experimental assessment of cycling ageing of lithium-ion second-life batteries from electric vehicles, J. Energy Storage 32 (2020), 101695.
[19] J. Liu, Q. Duan, K. Qi, Y. Liu, J. Sun, Z. Wang, Q. Wang, Capacity fading mechanisms and state of health prediction of commercial lithium-ion battery in total lifespan, J. Energy Storage 46 (2022), 103910.
[20] S.F. Schuster, T. Bach, E. Fleder, J. Müller, M. Brand, G. Sextl, A. Jossen, Nonlinear aging characteristics of lithium-ion cells under different operational conditions, J. Energy Storage 1 (2015) 44–53.
[21] M. Messing, T. Shoa, S. Habibi, Estimating battery state of health using electrochemical impedance spectroscopy and the relaxation effect, J. Energy Storage 43 (2021), 103210.
[22] M. Jafari, K. Khan, L. Gauchia, Deterministic models of li-ion battery aging: it is a matter of scale, J. Energy Storage 20 (2018) 67–77.
[23] C. Pastor-Fernández, K. Uddin, G.H. Chouchelamane, W.D. Widanage, J. Marco, A comparison between electrochemical impedance spectroscopy and incremental capacity-differential voltage as li-ion diagnostic techniques to identify and quantify the effects of degradation modes within battery management systems, J. Power Sources 360 (2017) 301–318.
[24] Y. Gao, J. Jiang, C. Zhang, W. Zhang, Z. Ma, Y. Jiang, Lithium-ion battery aging mechanisms and life model under different charging stresses, J. Power Sources 356 (2017) 103–114.
[25] Y. Li, K. Li, Y. Xie, B. Liu, J. Liu, J. Zheng, W. Li, Optimization of charging strategy for lithium-ion battery packs based on complete battery pack model, J. Energy Storage 37 (2021), 102466.
[26] C. Li, J. Li, J. Li, X. Zhang, T. Hou, Optimization strategy of secondary frequency modulation based on dynamic loss model of the energy storage unit, J. Energy Storage 51 (2022), 104425.
[27] M. Musallam, C.M. Johnson, An efficient implementation of the rainflow counting algorithm for life consumption estimation, IEEE Trans. Reliab. 61 (2012) 978–986.
[28] W. Vermeer, G.R.C. Mouli, P. Bauer, A comprehensive review on the characteristics and modelling of Lithium-ion battery ageing, IEEE Trans. Transp. Electrification 8 (2021) 2205–2232.
[29] I. San Martín, A. Berrueta, P. Sanchis, A. Ursúa, Methodology for sizing stand-alone hybrid systems: a case study of a traffic control system, Energy 153 (2018) 870–881.
[30] A. Soto, A. Berrueta, P. Sanchis, A. Ursúa, Analysis of the main battery characterization techniques and experimental comparison of commercial 18650 Li-ion cells, in: Proceedings - 2019 IEEE International Conference on Environment and Electrical Engineering and 2019 IEEE Industrial and Commercial Power Systems Europe, EEEIC/I&CPS Europe 2019, 2019, pp. 1–6.
[31] X. Han, L. Lu, Y. Zheng, X. Feng, Z. Li, J. Li, M. Ouyang, A review on the key issues of the lithium ion battery degradation among the whole life cycle, ETransportation 1 (2019), 100005.
[32] P. Shafiei Sabet, A.J. Warnecke, F. Meier, H. Witzenhausen, E. Martinez-Laserna, D. U. Sauer, Non-invasive yet separate investigation of anode/cathode degradation of lithium-ion batteries (nickel–cobalt–manganese vs. graphite) due to accelerated aging, J. Power Sources 449 (2020), 227369.
[33] T. Thien, H. Axelsen, M. Merten, D.U. Sauer, Energy management of stationary hybrid battery energy storage systems using the example of a real-world 5 MW hybrid battery storage project in Germany, J. Energy Storage 51 (2022), 104257.